Estuarine, Coastal and Shelf Science (2000) **50,** 49–58
Article No. ecss.1999.0531, available online at http://www.idealibrary.com on IDEAL®

The 1998 Coastal Turbidity Plume in Lake Michigan

D. J. Schwab[a,c], D. Beletsky[b] and J. Lou[a]

[a]*NOAA Great Lakes Environmental Research Laboratory, 2205 Commonwealth Blvd., Ann Arbor, MI 48105, U.S.A.*
[b]*Department of Naval Architecture and Marine Engineering, University of Michigan; Cooperative Institute for Limnology and Ecosystems Research/NOAA Great Lakes Environmental Research Laboratory and University of Michigan, Ann Arbor, MI 48105, U.S.A.*

Received 17 November 1998 and accepted in revised form 22 March 1999

In this paper, numerical models of coastal circulation, wind-waves, and sediment transport are applied to the March 1998 turbidity plume event in Lake Michigan to investigate the role of wind-induced circulation in the offshore transport of sedimentary material in Lake Michigan. Computer visualization is used to compare model results to the evidence of cross-isobath transport suggested in satellite imagery. Model results showed that circulation in Lake Michigan is highly episodic since it is almost entirely wind-driven in early spring. The characteristic wind-driven circulation pattern in the lake consists of two counter-rotating gyres, a counterclockwise-rotating gyre to the right of the wind, and a clockwise-rotating gyre to the left. The gyres are separated by a convergence zone along the downwind shore with resulting offshore flow and a divergence zone along the upwind shore with onshore flow. This two-gyre circulation pattern with offshore flow was very clearly seen during a northerly wind event in March 1998 in southern Lake Michigan. The strongest sediment resuspension occurred in the southern lake and the shallow waters along the coastline. This is because of the larger waves in southern Lake Michigan due to the dominant northerly wind in this early spring period. The two most significant sediment resuspension events were detected in the model results during the two storm events. Although results from the sediment transport model agree qualitatively with satellite imagery, they fail to simulate the initial eddy-like structure of the plume. Visualization is shown to be an effective tool for interpreting the complex turbidity patterns in the satellite imagery of the turbidity plume.

Keywords: sediment transport; numerical model; coastal currents; wind waves; visualization

Introduction

In the North American Great Lakes, as well as in the coastal ocean, the gradients of many biogeochemically important materials (BIMs) are considerably higher in the offshore direction than in the longshore direction (Brink *et al.*, 1992; Scavia & Bennett, 1980). In the presence of these large gradients, cross-isobath circulation is a primary mechanism for the exchange of material between nearshore and offshore waters. Both the alongshore and cross-isobath components of the current exhibit strong episodic behaviour due to wind forcing. As opposed to alongshore transport, the advective and diffusive mechanisms driving cross-isobath transport and the time scales over which they operate have not been extensively studied. A necessary step in understanding cross-isobath transport of BIMs is to identify and quantify the physical processes that are responsible for the nearshore-offshore water mass and material exchange. To this end, a multidisciplinary research program jointly sponsored by NOAA (National Oceanic and Atmospheric Administration) and NSF (National Science Foundation) was recently initiated to study the recurrent turbidity plume in southern Lake Michigan (http://www.glerl.noaa.gov/eegle).

In the context of nearshore–offshore transport, the Great Lakes present somewhat different challenges than the continental shelf. Although many of the physical processes responsible for the movement of material from the coastline toward deeper waters are similar in both environments, the fact that the lakes are fully enclosed by land has significant consequences. When material is transported offshore in the Great Lakes, it can only be removed from the system by permanent burial in the sediments or removal through an outflow. This is in contrast to the continental shelf where transport across the shelf break to the deep ocean can also be considered a removal mechanism. The physical mechanisms for cross-shelf transport are

Full sized figures, tables and animations are stored on the CD-ROM accompanying this article. Use a Web browser to access the start page ' default.htm ' and follow the links. The help file ' help.htm ' provides answers for some common problems.

[c]E-mail: schwab@zeus.glerl.noaa.gov

0272–7714/00/010049+10 $35.00/0

similar, and in some cases identical, to the processes that control nearshore-offshore transport in the lakes, but there is no analogue in the lakes for exchange with the deep ocean across the shelf break.

Recent satellite observations of suspended sedimentary material in Lake Michigan (Eadie *et al.*, 1996) offer a unique opportunity to investigate a recurrent episode of cross-isobath transport. A 10 km wide plume of resuspended material extending over 100 km along the southern shore of the lake was first observed in satellite imagery by Mortimer (1988), and has been observed every spring since 1992, when satellite imagery for the Great Lakes region first became available on a routine basis through the NOAA CoastWatch program (Schwab *et al.*, 1992). The bathymetry and geometry of the Lake Michigan basin are shown in Figure 1. The resuspension plume of March 1998 was one of the largest events of record. Satellite observations (Figure 2) reveal a well developed plume extending over 300 km of coastline from Milwaukee, WI (station MKE in Figure 1) to Muskegon, MI (station MKG in Figure 1) with several dominant offshore features originating from the south-eastern shoreline. The plume originated around March 10 following several days of intense storms that produced 17 m s^{-1} northerly winds and generated waves in the basin over 5 m high. Remnants of the plume feature were still observable by satellite six weeks later. Our current understanding is that the initiation of the plume is caused by a major storm with strong northerly winds generating large waves in southern Lake Michigan. The plume appears along the entire southern coastline of the lake. It occasionally veers offshore along the eastern shore of the lake, coincidentally near the areas of highest measured long-term sediment accumulation in the lake (Figure 3). The offshore structure of the turbidity plume often resembles the structure of cold water filaments seen in thermal imagery of the California Current by Strub *et al.* (1991) and others.

Considerable progress has recently been made in developing two and three dimensional circulation models for the Great Lakes. Numerical hydrodynamic models are now able to simulate large scale circulation in the lakes with reasonable accuracy (Schwab & Bedford, 1994; Beletsky *et al.*, 1997). It is possible to resolve kilometre scale variability in current and temperature fields with high resolution versions of these models. In addition, a parametric surface wind wave model developed by Schwab *et al.* (1984) is available for modelling waves at these same scales. This model has been shown to provide excellent estimates of wave height and wave direction for fetch-limited waves in several applications to the Great Lakes (Liu *et al.*, 1984; Schwab & Beletsky, 1998). Furthermore, a quasi-3-D suspended sediment transport model developed by Lou *et al.* (1999) has recently been coupled with the circulation and wind wave models to provide estimates of suspended sediment concentration at similar resolutions. In this paper, we apply the circulation, wind-wave, and sediment transport models to the March 1998 turbidity plume event in Lake Michigan to investigate the role of wind-induced circulation in the offshore transport of sedimentary material in Lake Michigan. Computer visualization is used to compare model results to the evidence of cross-isobath transport suggested in satellite imagery.

Wave model

The wave model is a numerical finite-difference solution to the two-dimensional wave momentum conservation equation. The wave energy spectrum is parameterized at each point on a rectilinear computational grid in terms of total wave energy, peak energy period, and predominant wave direction. The momentum balance equation is

$$\frac{\partial \boldsymbol{M}}{\partial t} + \boldsymbol{v}_g \nabla \boldsymbol{M} = \boldsymbol{\tau}_w$$

where ∇ is the horizontal gradient operator, and $\boldsymbol{M}$ and $\boldsymbol{v}_g$ are the total momentum vector and the corresponding group velocity vector, and $\boldsymbol{\tau}_w$ is that part of the momentum input from the wind that produces net wave momentum growth. The directional wave energy spectrum is assumed to have a cosine-squared angular dependence about a single dominant mean wave direction which is independent of frequency.

Momentum input from the wind consists of two components, one ($\boldsymbol{\tau}_1$) parallel to the wind vector and the other ($\boldsymbol{\tau}_2$) parallel to the wave momentum vector, i.e.

$$\boldsymbol{\tau}_w = \boldsymbol{\tau}_1 + \boldsymbol{\tau}_2$$

The scalar values of the two components as suggested by Donelan (1979) are:

$$\tau_1 = \frac{\gamma}{2} \rho_a D_1 |U - 0{\cdot}83 c_p \cos\theta_0| (U - 0{\cdot}83 c_p \cos\theta_0)$$

$$\tau_2 = \frac{\gamma}{2} \rho_a D_2 |U\cos\theta_0 - 0{\cdot}83 c_p| (U\cos\theta_0 - 0{\cdot}83 c_p)$$

where c_p is the wave phase velocity, ρ_a is the air density, U is the 10 m wind speed, θ_0 is the angle

between the wind and the waves, $\gamma(=0{\cdot}028)$ is the empirical fraction of the wind stress that is retained by the waves, and D_1 and D_2 are form drag coefficients given by

$$D_1=[0{\cdot}4/\ln(50/\xi\cos\theta_0)]^2$$

$$D_2=[0{\cdot}4/\ln(50/\xi)]^2$$

where ξ is the root mean square surface elevation (in metres). Both τ_1 and τ_2 may be positive, indicating wave growth, or negative, indicating wave decay.

To solve the momentum balance equation we use an empirical relationship between wave momentum and wave height derived from JONSWAP relations (Hasselman *et al.*, 1973) linking ξ^2 with peak energy frequency, f_p, and mean wind U:

$$\xi^2=6{\cdot}23\times10^{-6}\left(\frac{f_pU}{g}\right)^{-10/3}\frac{U^4}{g^2}$$

The model is thus semi-empirical and parametric. A simple numerical integration scheme can then be applied to the momentum balance equation. Forward time differences are used to calculate the momentum components at the centre of the grid squares, and a combination of upwind and centred differences are used to evaluate the momentum advection terms at the edges of the grid squares. Model output at each grid point consists of significant wave height (defined by $H_{1/3}=4\xi$), peak-energy wave period and average wave direction.

The model is applied on a 2 km rectilinear grid covering Lake Michigan. Output from the 2 km wave model (wave height and wave period) is used to estimate bottom shear stress in the sediment transport model described below.

Hydrodynamic model

A three-dimensional circulation model for the Great Lakes (Schwab & Beletsky, 1998) is used to calculate lake circulation. The model is based on the Princeton Ocean Model (Blumberg & Mellor, 1987) and is a nonlinear, fully three-dimensional, primitive equation, finite difference model. The model is hydrostatic and Boussinesq so that density variations are neglected except where they are multiplied by gravity in the buoyancy force. The model uses time-dependent wind stress and heat flux forcing at the surface, zero heat flux at the bottom, free-slip lateral boundary conditions, and quadratic bottom friction. The drag coefficient in the bottom friction formulation is spatially variable. It is calculated based on the assumption of a logarithmic bottom boundary layer using a constant bottom roughness of 1 cm.

To simplify the discussion of model physics, we present the dynamical equations in Cartesian co-ordinates. The velocity components (u,v,w) are in the (x,y,z) directions. The mass continuity equation is

$$\nabla\boldsymbol{V}+\frac{\partial w}{\partial z}=0$$

where $\mathbf{V}=(u,v)$ is the horizontal velocity. The horizontal momentum equations are

$$\frac{\partial u}{\partial t}+\boldsymbol{V}\nabla u+w\frac{\partial u}{\partial z}-fv=-\frac{1}{\rho_0}\frac{\partial p}{\partial x}+\frac{\partial}{\partial x}\left(A_M\frac{\partial u}{\partial x}\right)+\frac{\partial}{\partial y}\left(A_M\frac{\partial u}{\partial y}\right)+\frac{\partial}{\partial z}\left(K_M\frac{\partial u}{\partial z}\right)$$

$$\frac{\partial v}{\partial t}+\boldsymbol{V}\nabla v+w\frac{\partial v}{\partial z}+fu=-\frac{1}{\rho_0}\frac{\partial p}{\partial y}+\frac{\partial}{\partial x}\left(A_M\frac{\partial v}{\partial x}\right)+\frac{\partial}{\partial y}\left(A_M\frac{\partial v}{\partial y}\right)+\frac{\partial}{\partial z}\left(K_M\frac{\partial v}{\partial z}\right)$$

where ρ is density, p is pressure, f is the Coriolis parameter, and A_M and K_M are the horizontal and vertical momentum eddy viscosities, respectively. The Eulerian derivatives at a point are the result of the horizontal and vertical velocity advections, horizontal pressure gradient force, Coriolis force, and horizontal and vertical momentum diffusion. Horizontal diffusion is calculated with a Smagorinsky eddy parameterization (with a multiplier of 0·1) to give a greater mixing coefficient near strong horizontal gradients.

The Princeton Ocean Model employs a terrain following vertical co-ordinate system (σ- co-ordinate) which replaces the vertical co-ordinate, z, with a normalized vertical co-ordinate, $\sigma=(z-\eta)/(d+\eta)$, where d is the local depth, and η is the free surface elevation. The advantage of this system is that in the transformed co-ordinate system, the bottom corresponds to a uniform value of the vertical co-ordinate ($\sigma=-1$), thus simplifying the governing transport and continuity equations. The hydrodynamic model of Lake Michigan has 20 vertical levels and a uniform horizontal grid size of 2 km.

The equations are written in flux form, and the finite differencing is done on an Arakawa-C grid using a control volume formalism. The finite differencing scheme is second order and centred in space and time (leapfrog). The model includes the Mellor and Yamada (1982) level 2·5 turbulence closure parameterization for calculating the vertical mixing

coefficients for momentum K_M, and heat, K_H, from the variables describing the flow regime.

The output from the lake circulation model is used to provide estimates of horizontal advection and bottom shear stress for the sediment resuspension and transport model. In addition, the turbulence closure scheme in the circulation model can provide estimates of physical dispersion coefficients for water quality and toxics models.

Suspended sediment transport model

The suspended sediment transport model is a quasi-3-D model based on an asymptotic solution for uniform flow to the convection-diffusion equation as described by Galappatti and Vreugdenhil (1985). In the present model, this approach has been developed into more complicated flow fields and generalized to the combined wave-current situations.

The suspended particles are assumed to be so small that their motions relative to ambient fluid fall into Stokes' range. The basic equation describing mass conservation of suspended sediment in a turbulent flow can be expressed as:

$$\frac{\partial c}{\partial t}+u\frac{\partial c}{\partial x}+v\frac{\partial c}{\partial y}+(w-w_s)\frac{\partial c}{\partial z}=\frac{\partial}{\partial x}\left(\varepsilon_x\frac{\partial c}{\partial x}\right)+\frac{\partial}{\partial y}\left(\varepsilon_y\frac{\partial c}{\partial y}\right)+\frac{\partial}{\partial z}\left(\varepsilon_z\frac{\partial c}{\partial z}\right)$$

where ε_x, ε_y, ε_z are sediment particle diffusion coefficients in the x, y, z directions for the combined motion of waves and currents, and $c(x,y,z,t)$ is the suspended sediment concentration.

The wave effect is taken into account by assuming an analogy of mixing profile on a wave-averaged and turbulence-averaged scale and the modified eddy viscosity coefficient (Van Rijn, 1985), as well as by introducing an enhanced bottom shear stress (Lou & Ridd, 1996). In cases where suspended load is the main mode of sediment transport, an asymptotic solution of the convection-diffusion equation is presented. The vertical concentration structure has been shown to depend only on the vertical velocity profile and the mixing coefficient, and thus can be calculated in advance (Lou, 1995). As a result, the three-dimensional concentration problem is separated into two parts: a two-dimensional depth-averaged sediment concentration model and vertical concentration profiles being solved in advance.

The bottom shear stresses required by the sediment transport model for bottom boundary condition were calculated by a bottom boundary layer model. The effect of nonlinear wave-current interaction on the bottom shear stress was obtained based on the concept of Grant and Madsen (1979) in an iterative form (Lou & Ridd, 1997).

A three layer wave-induced diffusion coefficient (Van Rijn, 1986) was proposed in the sediment concentration model. The sediment mixing coefficient due to the combination of waves and current is assumed to be given by the sum of the squares of the current-related ($\varepsilon_{s,c}$) and wave-related ($\varepsilon_{s,w}$) values:

$$\varepsilon_s^2=\varepsilon_{s,c}^2+\varepsilon_{s,w}^2$$

The current-related turbulent eddy coefficient $\varepsilon_{s,c}$ is calculated numerically from the 3-D circulation model.

The bottom boundary conditions in the sediment transport model were evaluated at a reference water-sediment interface level $z=a$. The upward flux of suspended sediment at this reference level can be given by:

$$F_a=w_s(E_s-c_a\cos\theta)$$

where, c_a is the near bed concentration of suspended sediment, $w_s c_a \cos\theta$ is the deposition rate per unit bed area due to the fall velocity w_s, θ is the bottom slope and E_s is a dimensionless coefficient describing the entrainment of bottom sediment into suspension due to turbulence.

A similar entrainment coefficient described by Garcia and Parker (1991) was adopted in our study as follows:

$$E_s=\frac{AZ_k^5}{1+\frac{A}{0{\cdot}3}Z_k^5}$$

where

$$Z_k=\frac{u'_\star}{w_s}\left[\frac{\sqrt{(s-1)gD_k}}{v}D_k\right]^{0{\cdot}6}$$

A is a constant ($=1{\cdot}3\times10^{-7}$), s is the specific density, $u'_\star$ is the bottom shear velocity, D_k is the characteristic size of sediment, and v is the kinetic viscosity.

The suspended sediment concentration at reference level $z=a$ above the bed is expressed as (Van Rijn, 1989):

$$c_a=0{\cdot}015\frac{D_{50}}{a}\frac{T^{1{\cdot}5}}{D_\star^{0{\cdot}3}}$$

where

$$T=\frac{(\tau_b-\tau_{b,cr})}{\tau_{b,cr}}$$

τ_b is the effective bed shear stress under combined waves and current, and $\tau_{b,cr}$ the time-averaged Shields critical shear stress.

To reduce numerical dispersion, the second order upwind difference scheme has been applied to the horizontal advection terms. A hybrid Crank-Nicolson and ADI solution scheme is developed to calculate the concentration results. In the model application to Lake Michigan, a uniform 2 km horizontal grid mesh, 20 vertical layers, and a staggered C-grid arrangement were employed for the sediment transport model, which are compatible with the circulation and wind wave models mentioned above.

Forcing functions

To calculate momentum flux fields over the water surface for the lake circulation and wave models, it is necessary to estimate wind and air temperature fields at model grid points. Meteorological data were obtained from 12 National Weather Service stations around Lake Michigan (Figure 1). These observations form the basis for generating gridded overwater wind and air temperature fields.

Overland wind speeds generally underestimate overwater values because of the marked transition from high aerodynamic roughness over land to much lower aerodynamic roughness over water. This transition can be very abrupt so that wind speeds reported at coastal stations are often not representative of conditions only a few kilometres offshore. Schwab and Morton (1984) found that wind speeds from overland stations could be adjusted by empirical methods to obtain fair agreement with overlake wind speeds measured from an array of meteorological buoys in Lake Erie. For meteorological stations that are more representative of overland than overwater conditions, namely all stations except SGNW3 in Figure 1, the empirical overland-overlake wind speed adjustment from Resio and Vincent (1977) is applied.

To interpolate meteorological data observed at irregular points in time and space to a regular grid so that it can be used for input into numerical wave, sediment transport, and circulation models, some type of objective analysis technique must be used. For this study the nearest-neighbour technique was used, with the addition of a spatial smoothing step (with a specified smoothing radius). In the nearest neighbour technique, observations from up to three hours before the interpolation time to three hours after the interpolation time are also considered. In the nearest-neighbour distance calculations, the distance from a grid point to these observation points is increased by the product of the time difference multiplied by a scaling speed. The interpolation scaling speed is taken as $10\ \mathrm{km\ h^{-1}}$. Interpolation smoothing distance is 30 km. It was found that the nearest-neighbour technique provided results comparable to results from the inverse power law or negative exponential weighing functions discussed in Schwab (1989).

Results

Hourly meteorological data from the 12 stations shown in Figure 1 were obtained for the period 1–30 March, 1998. Overwater wind and air temperature fields were interpolated to the 2 km grid. Time series of wind speed and direction from a point in the middle of the southern basin (Figure 1) are shown in Figure 4. There are four major wind events in March, two storms with northerly winds (on the 9th and 21st) and two with southerly winds (on the 13th and 27th). In early spring, the lake is thermally homogeneous and density gradients are negligible. Therefore, the circulation model was applied in a barotropic mode with uniform (2 °C) water temperature. The wave model was used to compute hourly values of wave height, wave period, and wave direction, from which wave-induced bottom orbital velocity was calculated. The evolution of the computed wave height field for the 30 day simulation period is illustrated in Animation 1. Time series of wave model results for wave height, period, and direction at a point in the middle of the southern basin (Figure 1) are presented in Figure 4. The largest wave heights in the southern basin occur during the storms with northerly winds which provide the longest overwater fetch distance. The circulation model computed hourly values of horizontal currents and dispersion coefficients. The suspended sediment transport model then was used to simulate suspended sediment concentration during this period.

The computed circulation is illustrated through the use of a computer animation in Animation 2. The animation depicts the trajectories of passive tracer particles which were introduced into the computed depth-averaged velocity field on 1 March and are traced through the 30 day computational period. The mean wind vector is also shown. Particle trajectories are computed using the technique developed by Bennett *et al.* (1983) and Bennett and Clites (1987). This technique includes a method for interpolating the computed velocity field from velocity points on the computational grid to the particle locations, which minimizes collisions of the particles with the shoreline. Particles are initially located in the centre of every third grid cell. In order to more clearly illustrate the effect of lake circulation on cross-isobath transport,

particles initially placed in cells with depth less than 30 m are coloured orange in the animation.

In the animation a new visual technique is used to enhance the perception of fluid motion. Particle locations at each time step are depicted by a bright spot. Previous locations of that particle for the last 48 h are also depicted as spots of diminishing intensity. The visual effect is that of a ' tail ' on each particle whose length indicates the particle's speed and whose position indicates a history of the particle's recent locations. This technique is also useful for producing a ' snapshot ' of currents at a single time which also gives an indication of current magnitude and direction over the previous 48 h.

The time evolution of the modelled surface suspended sediment concentration in Lake Michigan is depicted in Animation 3. The model started from zero concentration over the whole lake as the initial condition on 1 March 1998. The dominant sediment particle size is assumed to be 15 μm, the settling velocity is set to 0·5 m day^{-1}, the critical bottom shear stress is 0·05 Nm^{-2}, and the bottom of the lake is treated as an unlimited sediment source. The animation shows colour contour maps of surface suspended sediment concentration at 3 h intervals. It illustrates the hydrodynamic effects on sediment resuspension and transport resulting from the interactions among sediment, topography, circulation and wind waves in Lake Michigan.

A simple estimation of sediment erosion and deposition is made based on the sediment transport results in March 1998, with the purpose of highlighting the hydrodynamic effects on sediment redistribution in the lake. During the course of model simulation, the sediment layer thickness changes with sediment erosion from the bottom or deposition from the water column. The erosion and deposition areas were determined by comparing the final sediment layer thickness with the initial thickness. The net change in bed thickness resulting from the March 1998 simulation is given in Figure 7.

Discussion

Model results showed that circulation in Lake Michigan is highly episodic since it is almost entirely wind-driven in early spring. The characteristic wind-driven circulation pattern in a lake consists of two counter-rotating gyres: a counterclockwise-rotating (cyclonic) gyre to the right of the wind and a clockwise-rotating (anticyclonic) gyre to the left (Bennett, 1974). The gyres are separated by a convergence zone along the downwind shore with resulting offshore flow and a divergence zone along the upwind shore with onshore flow. This two-gyre circulation pattern was very clearly seen during several wind events in March in southern Lake Michigan (Animation 2 and Figure 5). The first storm with northerly winds up to 17 m s^{-1} on 9 March caused strong along-shore southerly currents that converged near Benton Harbor, Michigan (station BEH in Figure 1) and caused massive offshore flow lasting several days. The second northerly storm on 21 March also produced a two-gyre circulation pattern in southern Lake Michigan, but with a cyclonic gyre which was more prominent than the anticyclonic gyre. Finally, southerly winds on 26–27 March created a ' reversed ' two-gyre circulation pattern with onshore flow near Benton Harbor instead of offshore flow. We were not able to reproduce the spectacular spiral eddy observed in the middle of the lake on 12 March (Figure 2) which is probably a result of meandering of the strong offshore jet.

Sediment concentration results showed that at least some suspended sediment was present during most days of March 1998 (Figure 6 and Animation 3). The strongest sediment resuspension mainly occurred in the southern lake and the shallow waters near the coastline. This is caused by the larger waves in southern Lake Michigan due to the dominant northerly wind in this early spring period. The two most significant sediment resuspension events were detected in the model results on 9–12 March and 20–22 March, which coincide with the strongest northerly winds as shown in Figure 4.

The first storm caused strong sediment resuspension (with concentration values above 10 mg l^{-1}) in coastal areas within the 30 m isobath after 8 March (Animation 3). Large waves (over 5 m) were responsible for the local resuspension along the coastline and mid-lake ridge area, and the strong currents determined the plume advection. The most significant activity occurred along the southern and south-eastern shoreline during 10–12 March and 21–23 March. The sediment model was not able to simulate the observed offshore spiral eddy structure on 12 March. The second resuspension event also occurred under northerly wind conditions on 21 March. The sediment concentration results showed a similar pattern but with somewhat smaller magnitudes. Another noticeable phenomenon in the model results is evidence of high offshore suspended sediment concentration near the south-eastern corner of the lake during the 9–12 March storm, and a similar pattern after 21 March. From the circulation model results (Figure 5 and Animation 2), it is clearly seen that this high offshore sediment concentration coincided with strong offshore flow, which may have moved the

material from the coastal area to the deeper waters. Similar offshore sediment transport was also seen in previous plume events, with the offshore flow occurring at slightly different sites along the south-eastern shoreline depending on wind direction. Since the area of high offshore sediment concentration also coincides with an area of strong currents, the high sediment concentration in the model may also be caused by local resuspension rather than advection or diffusion.

As shown in Figure 7, net erosion during the storm events in March 1998, occurred mainly along the shoreline and deposition occurred offshore. Overall, the deposition pattern during this event is similar to the long term sediment accumulation map shown in Figure 3. Both show an asymmetric pattern of sediment deposition, with maximum deposition occurring mainly in the eastern side of the lake in water depths of 50–100 m. This asymmetric pattern was basically established after the first wind event and did not change much during the rest of the month, which tends to support the hypothesis that the long term sediment deposition pattern may be largely determined by a few major storm events. The largest net deposition occurred in the southern and south-eastern part of the lake and around the mid-lake ridge area. The net sediment accumulation in the southern lake is consistent with the circulation convergence zone and its extension offshore, where the sediment particles suspended by the high erosion along the western and eastern shores were probably transported by the large offshore currents. The greatest erosion occurred along the western shore and also in the mid-lake ridge area. Given that the bottom sediment dry bulk density is 1450 kg m^{-3}, the estimated total resuspended sediment mass in March 1998 in Lake Michigan was $7{\cdot}53 \times 10^9$ kg.

Though the sediment transport model can depict the resuspension events reasonably well, it was not able to describe the detailed plume structure, particularly the spiral eddy in the central part of southern lake. Because the offshore structure of the sediment plume depends strongly on the circulation patterns, we believe that inaccuracies in the hydrodynamic model results could well be responsible for the missing features. To study this unique process further, more hydrodynamic and sediment transport studies are needed in the future. More experiments are underway to study effects of wind field interpolation, grid resolution, and friction on hydrodynamics and sediment dynamics in Lake Michigan.

Acknowledgements

This is GLERL Contribution No. 1124. This work is part of the EEGLE (Episodic Events—Great Lakes Experiment) Program sponsored by the National Science Foundation and the National Oceanic and Atmospheric Administration Coastal Ocean Program. J.L. was supported by the National Research Council's Research Associateship Program.

References

Beletsky, D., O'Connor, W. P., Schwab, D. J. & Dietrich, D. E. 1997 Numerical simulation of internal Kelvin waves and coastal upwelling fronts. *Journal of Physical Oceanography* **27,** 1197–1215.

Bennett, J. R. 1974 On the dynamics of wind-driven lake currents. *Journal of Physical Oceanography* **4,** 400–414.

Bennett, J. R., Clites, A. H. & Schwab, D. J. 1983 A two-dimensional lake circulation modeling system: programs to compute particle trajectories and the motion of dissolved substances. *NOAA Tech. Memo. ERL GLERL-46*. NOAA Great Lakes Env. Res. Lab., Ann Arbor, MI, 51 pp.

Bennett, J. R. & Clites, A. H. 1987 Accuracy of trajectory calculation in a finite-difference circulation model. *Journal of Computational Physics* **68,** 272–282.

Blumberg, A. F. & Mellor, G. L. 1987 A description of a three-dimensional coastal ocean circulation model. In *Three dimensional Coastal Ocean Models, Coastal and Estuarine Sciences* 5 (Heaps, N. S., ed.), American Geophysical Union, Washington D.C., pp. 1–16.

Brink, K. H., Bane, J. M., Church, T. M., Fairall, C. W., Geernaert, G. L., Hammond, D. E., Henrichs, S. M., Martens, C. S., Nittrouer, C. A., Rogers, D. P., Roman, M. R., Roughgarden, J. D., Smith, R. L., Wright, L. D. & Yoder, J. A. 1992 *Coastal Ocean Processes: A Science Prospectus. Rept. No. WHOI-92-18*, Woods Hole Oceanographic Institution, Woods Hole, MA. 103.

Donelan, M. A. 1979 On the fraction of wind momentum retained by waves. In *Marine Forecasting, Predictability and Modeling in Ocean Hydrodynamics* (Nihoul, J. C., ed.), Elsevier, Amsterdam, pp. 141–159.

Eadie, B. J., Schwab, D. J., Leshkevich, G. L., Johengen, T. H., Assel, R. A., Holland, R. E., Hawley, N., Lansing, M. B., Lavrentyev, P., Miller, G. S., Morehead, N. R., Robbins, J. A. & Van Hoof, P. L. 1996 Anatomy of a recurrent episodic event: a winter-spring plume in southern Lake Michigan *EOS. Transactions of the American Geophysical Union* **77,** 337–338.

Foster, D. S. & Colman, S. M. 1992 *Thickness and Distribution of Post Glacial Deposits Beneath Lake Michigan*. US Geological Survey Miscellaneous Field Map, MI-2202.

Galappatti, G. & Vreugdenhil, C. B. 1985 A depth-integrated model for suspended sediment transport. *Journal of Hydraulic Research* **23,** 359–376.

Garcia, M. H. & Parker, G. 1991 Entrainment of bed sediment into suspension. *Journal of Hydraulic Engineering* **117,** 414–435.

Grant, W. D. & Madsen, O. S. 1979 Combined wave and current interaction with a rough bottom. *Journal of Geophysical Research* **84,** 1797–1808.

Hasselmann, K., Barnett, T. P., Bouws, E., Carlson, H., Cartwright, D. E., Enke, K., Ewing, J. A., Gienapp, H., Hasselmann, D. E., Kruseman, P., Merrburg, A., Muller, P., Olbers, D. J., Richter, K., Sell, W. & Walden, H. 1973 Measurements of wind-wave growth and swell decay during the Joint North Sea Wave Project (JONSWAP). *Deutsche Hydrographische Zeitschrift* **A12,** 95.

Liu, P. C., Schwab, D. J. & Bennett, J. R. 1984 Comparison of a two-dimensional wave prediction model with synoptic measurements. *Journal of Physical Oceanography* **14,** 1514–1518.

Lou, J. 1995 *Modelling of Hydrodynamics and Suspended Sediment Transport in Coastal Areas*. Ph.D Thesis, James Cook University, Australia.

Lou, J. & Ridd, P. 1996 Wave-current bottom shear stresses and sediment resuspension in Cleveland Bay, Australia. *Coastal Engineering* **29,** 169–186.

Lou, J. & Ridd, P. 1997 Modeling of suspended sediment transport in coastal areas under waves and current. *Estuarine, Coastal and Shelf Science* **45,** 1–16.

Lou, J., Schwab, D. J. & Beletsky, D. 1999 A model of sediment resuspension and transport dynamics in southern Lake Michigan. *Journal of Geophysical Research* (in press).

Mellor, G. L. & Yamada, T. 1982 Development of a turbulence closure model for geophysical fluid problems. *Reviews of Geophysics and Space Physics* **20,** 851–875.

Mortimer, C. H. 1988 Discoveries and testable hypotheses arising from Coastal Zone Color Scanner imagery of southern Lake Michigan. *Limnology and Oceanography* **33,** 203–226.

Resio, D. T. & Vincent, C. L. 1977 Estimation of winds over the Great Lakes. *Journal of the Waterway, Port, and Coastal Ocean Division, ASCE* **102,** 265–283.

Scavia, D. & Bennett, J. R. 1980 Spring transition period in Lake Ontario - a numerical study of the causes of the large biological and chemical gradients. *Canadian Journal of Fisheries and Aquatic Science* **37,** 823–833.

Schwab, D. J. 1989 The use of analyzed wind fields from the Great Lakes marine observation network in wave and storm surge forecast models. *Preprint Volume of the 2nd International Workshop on Wave Hindcasting and Forecasting.* Environment Canada, Atmos. Env. Service, Downsview, Ont. pp. 257–266.

Schwab, D. J. & Bedford, K. W. 1994 Initial implementation of the Great Lakes Forecasting System: a real-time system for predicting lake circulation and thermal structure. *Water Pollution Research Journal of Canada* **29,** 203–220.

Schwab, D. J. & Beletsky, D. 1998 *Lake Michigan Mass Balance Study: Hydrodynamic modeling project. NOAA Tech. Memo. ERL GLERL-108.* NOAA Great Lakes Env. Res. Lab., Ann Arbor, MI, 53 pp.

Schwab, D. J., Bennett, J. R., Liu, P. C. & Donelan, M. A. 1984 Application of a simple numerical wave prediction model to Lake Erie. *Journal of Geophysical Research* **89,** 3586–3589.

Schwab, D. J. & Morton, J. A. 1984 Estimation of overlake wind speed from overland wind speed: a comparison of three methods. *Journal of Great Lakes Research* **10,** 68–72.

Schwab, D. J., Leshkevich, G. A. & Muhr, G. C. 1992 Satellite measurements of surface water temperature in the Great Lakes: Great Lakes Coast Watch. *Journal of Great Lakes Research* **18,** 247–258.

Strub, P. T., Kosro, P. M. & Huyer, A. 1991 The nature of cold filaments in the California Current System. *Journal of Geophysical Research* **96,** 14743–14768.

Van Rijn, L. C. 1985 *Two-dimensional vertical mathematical model for suspended sediment transport by currents and waves. Rep. S488-IV*, Delft Hydraulics Lab.

Van Rijn, L. C. 1986 Mathematical modeling of suspended sediment in nonuniform flows. *Journal of Hydraulic Engineering* **112,** 433–455.

Van Rijn, L. C. 1989 *Sediment transport by currents and waves. Rep. H461*, Delft Hydraulics Lab.

FIGURE 1. Geometry and bathymetry of Lake Michigan showing 2 km computational grid, metrological stations, and location of mid-lake station in southern Lake Michigan.

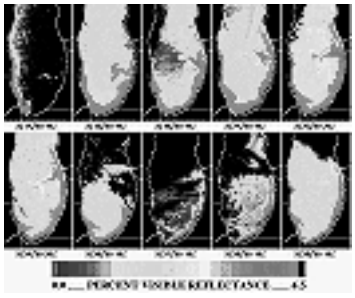

FIGURE 2. Satellite measurements of surface reflectance in southern Lake Michigan.

FIGURE 3. Long term sediment accumulation in southern Lake Michigan (Foster & Colman, 1992). The five ranges of sediment thickness depicted in the map are (from lightest to darkest): 1–2 m, 2–6 m, 6–10 m, 10–14 m, and >14 m. Labelled bathymetric contours are in metres.

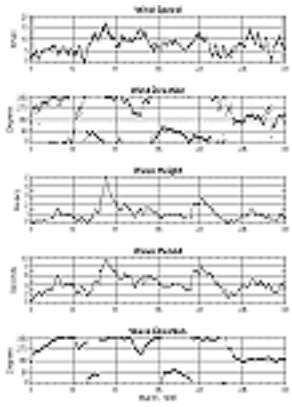

FIGURE 4. Time series of interpolated wind and modelled waves at a location in the centre of southern Lake Michigan for 1–30 March, 1998.

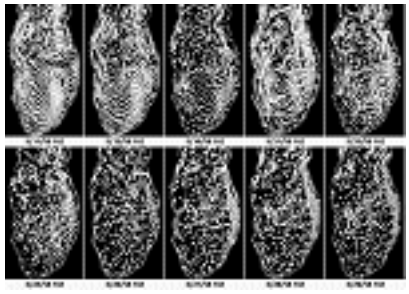

FIGURE 5. Snapshots of particle trajectory animation at times corresponding to satellite images in Figure 2.

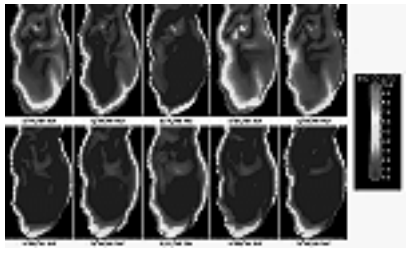

FIGURE 6. Snapshots of suspended sediment concentraiton animation at times corresponding to satellite images in Figure 2.

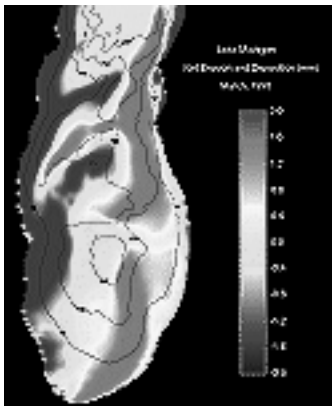

FIGURE 7. Net sediment erosion or depostion calculated from the sediment transport odel during March 1998. The positive values (red) represent depostion, and the negative values (blue) show erosion in mm.

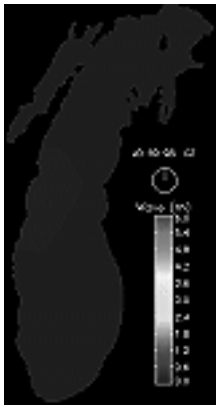

ANIMATION 1. Modelled significant wave height in Lake Michigan for 1–30 March, 1998.

ANIMATION 2. Modelled particle trajectories in Lake Michigan for 1–30 March, 1998.

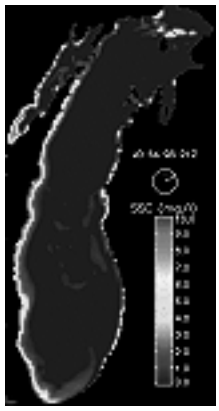

ANIMATION 3. Modelled surface suspended sediment concentration in Lake Michigan for 1–30 March, 1998.